Available online at www.sciencedirect.com
SCIENCE DIRECT®
International Journal of Heat and Mass Transfer 47 (2004) 4733–4744
International Journal of HEAT and MASS TRANSFER
www.elsevier.com/locate/ijhmt

Three-dimensional thermal analysis of heat sinks with circular cooling micro-channels

C.J. Kroeker, H.M. Soliman *, S.J. Ormiston

Department of Mechanical and Industrial Engineering, University of Manitoba, Winnipeg, Manitoba, Canada R3T 5V6

Received 5 March 2004; received in revised form 21 May 2004

Abstract

The pressure drop and thermal characteristics of heat sinks with circular micro-channels are investigated using the continuum model consisting of the conventional Navier–Stokes equations and the energy conservation equation. Developing flow (both hydrodynamically and thermally) is assumed in the fluid region and three-dimensional conjugate heat transfer is assumed in the solid region. Thermal results based on this approach are shown to be in good agreement with existing experimental data. Effects of various geometrical parameters, material properties, and Reynolds number on the thermal performance of the sink were investigated. A comparison between circular and rectangular channels at the same Reynolds number and hydraulic diameter showed that sinks with rectangular channels have lower thermal resistance, while sinks with circular channels dissipate more heat per unit pumping power.

Keywords: Micro-channels; Circular; Thermal performance; Three-dimensional; Conjugate; Numerical

1. Introduction

The steady demand for continuous enhancement in the performance of electronic products requires the development of efficient and compact heat dissipation devices. Electronic packages are required to operate at increasingly elevated heat fluxes and must be maintained below given design temperatures for stable and reliable operation. An innovative method for removing large amounts of heat from small areas is the micro-channel heat sink. This cooling device is made from highly conductive solid (e.g., silicon or copper) with micro-channels machined in it and used as flow passages for the cooling fluid. Recent advances in micro-fabrication techniques have facilitated the construction of these devices [1].

Successful design of micro-channel heat sinks requires fundamental understanding of the transport processes involved. A major issue that received considerable attention in the recent literature is whether the continuum/classical model (the conventional Navier–Stokes equations and the conventional energy equation) is valid at the micro-scale. Adams et al. [2] reported experimental data for turbulent, forced convection of water in circular micro-channels with diameters of 0.76 and 1.09 mm. They noted that the classical correlations for Nusselt number under-predicted the measured values and they proposed a specialized correlation for micro-channels. However, more recently, a similar experiment was performed by Owhaib and Palm [3] in which turbulent

* Corresponding author. Tel.: +1 204 474 9307; fax: +1 204 275 7507.
E-mail address: hsolima@cc.umanitoba.ca (H.M. Soliman).

0017-9310/$ - see front matter © 2004 Elsevier Ltd. All rights reserved.
doi:10.1016/j.ijheatmasstransfer.2004.05.028

Nomenclature

A_c	cross-sectional area (m^2)
B	width of cross-sectional cell containing one micro-tube (m)
B_T	total width of heat sink (m)
C_p	specific heat at constant pressure ($J\,kg^{-1}\,K^{-1}$)
D	diameter of micro-tube (m)
f	friction factor defined by Eq. (9)
H	thickness of the heat sink (m)
k	thermal conductivity ($W\,m^{-1}\,K^{-1}$)
L	length of the heat sink (m)
N	number of parallel channels in the heat sink
Nu	Nusselt number defined by Eq. (14)
P	dimensionless pressure defined by Eq. (7c)
p	pressure (Pa)
P_{WR}	pumping power (W)
Pr	Prandtl number defined by Eq. (7d)
q''	input heat flux ($W\,m^{-2}$)
q_z	heat rate gained by coolant per unit length ($W\,m^{-1}$)
Re	Reynolds number defined by Eq. (7d)
S	distance between centerline of micro-tube and heated surface of the sink (m)
T	temperature (K)
U	dimensionless velocity component in the x direction defined by Eq. (7b)
u	velocity component in the x direction ($m\,s^{-1}$)
V	dimensionless velocity component in the y direction defined by Eq. (7b)
v	velocity component in the y direction ($m\,s^{-1}$)
W	dimensionless velocity component in the z direction defined by Eq. (7b)
w	velocity component in the z direction ($m\,s^{-1}$)
w_m	mean velocity in the z direction ($m\,s^{-1}$)
X, Y, Z	dimensionless Cartesian coordinates defined by Eq. (7a)
x, y, z	Cartesian coordinates (m)

Greek symbols

Γ	dimensionless overall thermal resistance defined by Eq. (17)
γ	overall thermal resistance ($K\,W^{-1}$)
ϕ	angular position around the micro-channel measured clockwise from the top (radians)
θ	dimensionless temperature defined by Eq. (7c)
μ	dynamic viscosity ($N\,s\,m^{-2}$)
ρ	density ($kg\,m^{-3}$)

Subscripts

av	average value
b	bulk
f	fluid
i	solid–fluid interface
in	at inlet of channel
out	at outlet of channel
s	solid
z	in the z direction

forced convection of R-134a was investigated in a single micro-tube (0.8, 1.2, or 1.7 mm i.d.). Their results showed good agreement with the classical correlations, while none of the specialized correlations, including the one in [2], agreed with the test data. Guo and Li [4] argued that discrepancies between the experimental results for micro-channels and the classical correlations might be due to measurement errors and should not be misunderstood as being caused by novel phenomena at the micro-scale. In order to examine the range of applicability of the classical laws at the micro-scale, Gao et al. [5] measured the pressure-drop and heat-transfer characteristics of two-dimensional, parallel-plate micro-channels with gap sizes ranging from 0.1 to 1 mm using water as the test fluid. Their measurements of the overall friction coefficient and local Nusselt number showed that the classical laws of hydrodynamics and heat transfer are valid for gap sizes of 0.5 mm or higher. There was a departure between the data in [5] and the classical laws for gap sizes less than 0.5 mm.

Fedorov and Viskanta [6], and later Qu and Mudawar [7] presented numerical results for the detailed temperature and heat flux distributions in a heat sink with rectangular micro-channels (57 μm wide×180 μm deep). The continuum model was used and the problem was formulated for three-dimensional conjugate heat transfer in both investigations. The continuum model was proven to be valid by showing that the numerical results for the friction factor and overall thermal resistance of the heat sink were in good agreement with the experimental results of Kawano et al. [8]. Toh et al. [9] followed a similar approach and demonstrated that the numerical results from the continuum model using a three-dimensional conjugate approach agreed well with experimental results reported by Tuckerman [10]. Qu and Mudawar [11] reported both experimental and numerical results for the pressure drop and heat transfer in a heat sink with rectangular micro-channels (231 μm wide×713 μm deep). Again, they noted that the continuum model predicted the fluid flow and heat transfer

characteristics fairly well at the micro-scale. Ambatipudi and Rahman [12] performed a numerical simulation of three-dimensional, conjugate heat transfer in heat sinks with rectangular micro-channels. They investigated the effects of channel width, channel depth, the number of channels, and Reynolds number on the thermal performance of the heat sink. They reported good agreement between their numerical simulations and the experimental results of Harms et al. [13].

Other studies involving one or more simplifying assumptions were reported on heat sinks with rectangular micro-channels. Weisberg et al. [14] solved the fluid flow and heat transfer problems numerically assuming fully developed flow both hydrodynamically and thermally. Tunc and Bayazitoglu [15] adopted that same assumption and, in addition, assumed constant wall heat flux both axially and circumferentially. They then solved the model using the integral transform technique. Mala and Li [16] measured the pressure drop of water in micro-tubes (50–254 μm in diameter) and compared their results with the conventional theory for fully developed conditions. They noted that the measured values were always higher than the numerical values; however, it is not clear whether the deviation is because the conventional theory is not valid or because of the assumption of fully developed flow in the theory. Ryu et al. [17] assumed fully developed hydrodynamics and developing heat transfer. They solved numerically for the geometrical parameters that will minimize the overall thermal resistance for given pumping power.

All the above theoretical analyses correspond to micro-channels of rectangular cross-section. The objective of this study is to extend the analysis to heat sinks with circular micro-channels by exploring the fundamental features of the thermal behavior of such devices. The continuum model will be applied and numerical solutions will be obtained using a rigorous three-dimensional conjugate heat transfer approach. Validity of the approach will be confirmed by comparisons with available experimental data. A parametric study will be conducted in order to examine the effect of geometry on the thermal behavior of the heat sink. As well, a comparison will be made between the overall performances of heat sinks with rectangular micro-channels and sinks with circular micro-channels in order to relate the present study to earlier research.

2. Analysis

2.1. Geometry and flow conditions

A schematic diagram of the heat sink, with length L and total width B_T, is shown in Fig. 1(a). The electronic component is simulated as a constant heat flux (q'') at the top wall of the sink. All other surfaces of the heat sink are assumed insulated. Liquid coolant enters the micro-tubes with a uniform velocity w_m and a uniform temperature T_{in}. The flow is assumed laminar and steady and the fluid is assumed incompressible. Viscous dissipation and natural convection are assumed to be negligible. Constant properties are assumed in the fluid and solid regions. The magnitude of temperature changes within the solution domain does not justify the need for using temperature-dependent properties in the simulations. All previous analyses used the constant-properties assumption [6,7,9,11,12,14].

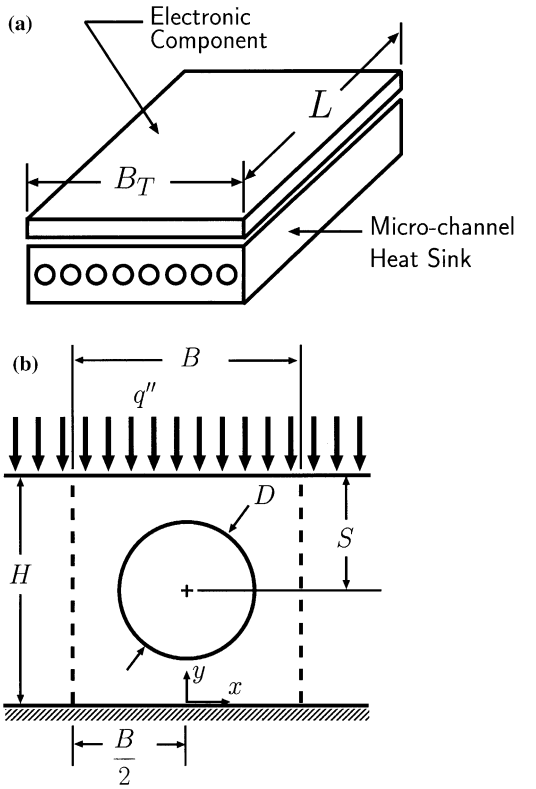

Fig. 1. (a) Schematic diagram of heat sink. (b) Schematic diagram of a unit cell.

From geometrical symmetry, a unit cell consisting of one micro-tube and the surrounding solid can be identified, as shown in Fig. 1(b). Moreover, $x = 0$ is also a symmetry plane so that only half of the unit cell needs to be solved. The relevant geometry parameters are the height H, the unit-cell width B, the channel diameter D, and the distance from the top surface to the centre of the micro-channel S. Coordinates x and y are shown in Fig. 1(b), while z is in the flow direction along the channel.

Fluid flow at the exit of the channel ($z = L$) is expected to be still developing, both thermally and hydrodynamically, and therefore the boundary conditions at this location are not known a priori. An additional

circular channel section of length $2L$ with an adiabatic outer surface was added to the flow channel at the exit of the heat sink and this length was found to be sufficient to establish fully developed hydrodynamics and a uniform temperature for all the conditions that were tested in this study.

2.2. Governing equations and boundary conditions

Based on the above assumptions, the non-dimensional governing equations in the fluid region can be written as:

$$\frac{\partial U}{\partial X}+\frac{\partial V}{\partial Y}+\frac{\partial W}{\partial Z}=0 \tag{1}$$

$$U\frac{\partial U}{\partial X}+V\frac{\partial U}{\partial Y}+W\frac{\partial U}{\partial Z} =-\frac{1}{2}\frac{\partial P}{\partial X}+\left(\frac{1}{Re}\right)\left(\frac{\partial^2 U}{\partial X^2}+\frac{\partial^2 U}{\partial Y^2}+\frac{\partial^2 U}{\partial Z^2}\right) \tag{2}$$

$$U\frac{\partial V}{\partial X}+V\frac{\partial V}{\partial Y}+W\frac{\partial V}{\partial Z} =-\frac{1}{2}\frac{\partial P}{\partial Y}+\left(\frac{1}{Re}\right)\left(\frac{\partial^2 V}{\partial X^2}+\frac{\partial^2 V}{\partial Y^2}+\frac{\partial^2 V}{\partial Z^2}\right) \tag{3}$$

$$U\frac{\partial W}{\partial X}+V\frac{\partial W}{\partial Y}+W\frac{\partial W}{\partial Z} =-\frac{1}{2}\frac{\partial P}{\partial Z}+\left(\frac{1}{Re}\right)\left(\frac{\partial^2 W}{\partial X^2}+\frac{\partial^2 W}{\partial Y^2}+\frac{\partial^2 W}{\partial Z^2}\right) \tag{4}$$

$$U\frac{\partial \theta}{\partial X}+V\frac{\partial \theta}{\partial Y}+W\frac{\partial \theta}{\partial Z} =\left(\frac{1}{RePr}\right)\left(\frac{\partial^2 \theta}{\partial X^2}+\frac{\partial^2 \theta}{\partial Y^2}+\frac{\partial^2 \theta}{\partial Z^2}\right) \tag{5}$$

The dimensionless energy equation in the solid is

$$\frac{\partial^2 \theta_s}{\partial X^2}+\frac{\partial^2 \theta_s}{\partial Y^2}+\frac{\partial^2 \theta_s}{\partial Z^2}=0 \tag{6}$$

where

$$X=\frac{x}{D},\quad Y=\frac{y}{D},\quad Z=\frac{z}{D} \tag{7a}$$

$$U=\frac{u}{w_m},\quad V=\frac{v}{w_m},\quad W=\frac{w}{w_m} \tag{7b}$$

$$P=\frac{p-p_{in}}{\frac{1}{2}\rho w_m^2},\quad \theta=\frac{T-T_{in}}{q''B/k_s} \tag{7c}$$

$$Re=\frac{\rho w_m D}{\mu},\quad Pr=\frac{\mu C_p}{k} \tag{7d}$$

The boundary conditions are:

$$\frac{\partial \theta}{\partial X}=\frac{\partial \theta_s}{\partial X}=0 \text{ at } X=0 \quad \text{and} \quad \frac{\partial \theta_s}{\partial X}=0 \text{ at } X=B/(2D) \tag{8a}$$

$$\frac{\partial \theta_s}{\partial Y}=0 \text{ at } Y=0 \quad \text{and} \quad \frac{\partial \theta_s}{\partial Y}=\frac{D}{B} \text{ at } Y=H/D \tag{8b}$$

$$U=V=\theta=0 \text{ and } W=1 \text{ (in the fluid)} \quad \text{and} \quad \frac{\partial \theta_s}{\partial Z}=0 \text{ (in the solid) at } Z=0 \tag{8c}$$

$$\frac{\partial \theta_s}{\partial Z}=0 \quad \text{at } Z=L/D \tag{8d}$$

$$U=V=\frac{\partial W}{\partial Z}=\frac{\partial \theta}{\partial Z}=0 \quad \text{at } Z=3L/D \tag{8e}$$

In addition to the above conditions, zero velocities and continuity of temperature and heat flux were imposed at the fluid–solid interface.

The mathematical model given by Eqs. (1)–(6) and boundary conditions (8a)–(8e) indicates that values of U, V, W, P, and θ (or θ_s) at any point (X,Y,Z) are dependent on the geometry parameters B/D, H/D, L/D, and S/H, the flow parameter Re, and the property parameters Pr and k_s/k_f. The variable k_s/k_f arises from imposing the equality of heat flux at the solid-fluid interface. The numerical value of D should not matter as long as the continuum model is applicable.

3. Numerical solution

Numerical solution of the above model was obtained using a finite-control-volume method [18], together with a finite-element approach of representing the geometry. Cartesian velocity components were used on a non-staggered, structured, multi-block grid. Mass conservation discretization on the non-staggered grid was based on an adaptation of earlier techniques [19,20]. The discretized mass and momentum conservation equations were fully coupled and solved simultaneously using additive correction multi-grid to accelerate convergence. Double precision was used in the computations and solutions were considered converged when the sum of the absolute dimensionless residuals of the discretized equations was less than 1.0×10^{-7}.

A block structured computational mesh was created. An example of a coarse mesh in the x–y plane is shown in Fig. 2. In this plane, the mesh consisted of uniformly spaced grid divisions in a rectangular region around the center of the circular channel. Outside the rectangular region, the grid contracted geometrically towards the interface between the fluid and the solid. Uniform spacing was used in the solid region in the x–y plane. Along the z-axis, the mesh expanded geometrically for the distance L. Uniform axial-grid spacing was used in the additional adiabatic length of $2L$ that was added to the circular-channel region past the end of the solid region. This additional length permitted placing outflow boundary conditions of fully developed velocity and

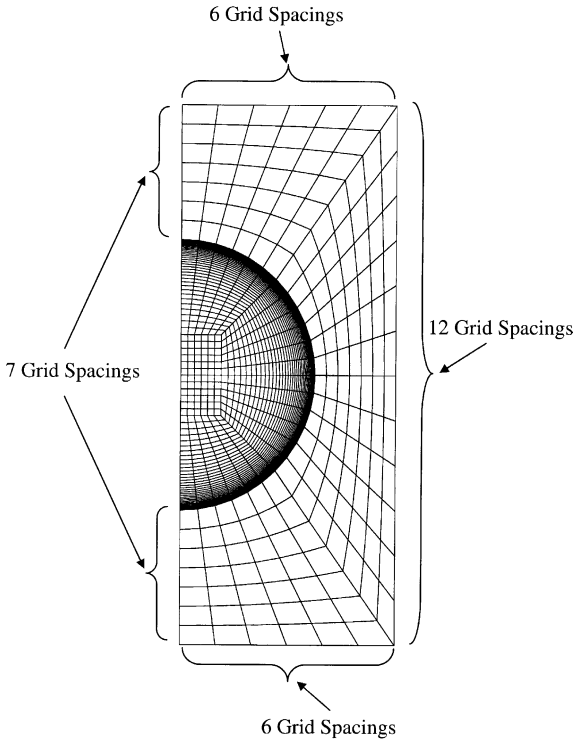

Fig. 2. A sample of the cross-sectional grid.

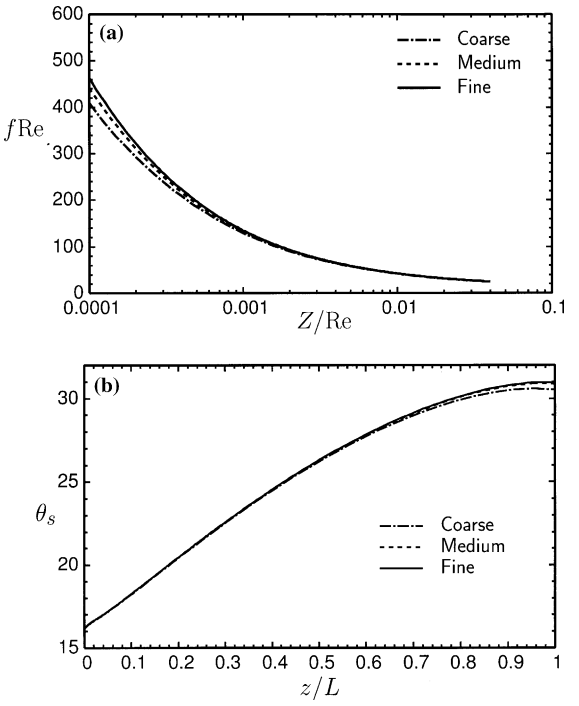

Fig. 3. (a) Axial variation of fRe for three different mesh sizes. (b) Axial variation of wall temperature for three different mesh sizes.

uniform temperature at $z = 3L$, rather than assuming fully developed conditions in the channel at $z = L$. Further details of the numerical approach can be found in [21].

3.1. Mesh independence and code validation

Grid-independence tests were conducted by generating results for two heat sinks of different geometry using three mesh sizes in each case. These three meshes were labeled coarse (100 axial subdivisions×580 subdivisions in each axial cross-section), medium (200×1252) and fine (300×1642). Samples of these results (corresponding to $L/D = 20$, $B/D = 1.2$, $H/D = 2.0$, $S/H = 0.5$, $Re = 500$, $Pr = 7$, and $k_s/k_f = 668.3$) are shown in Fig. 3(a) and (b).

Fig. 3(a) shows the predicted variation of fRe along the heat sink, where the friction factor f is defined by

$$f = -P_{av}/(4Z) \tag{9}$$

where P_{av} is the cross-sectional average dimensionless pressure. Fig. 3(a) shows that the deviation between the coarse and fine meshes is significant at low values of Z/Re, while the deviation between the medium and fine meshes is relatively smaller (maximum deviation is 4.4% at $Z/Re = 1\times10^{-4}$). Fig. 3(b) shows the variation of wall temperature along z for $x = 0$ and $y = H$. The sharp jump in θ_s near $z = 0$ is consistent with the results in [6,7,11]. Again, there is some deviation between the predictions of the coarse and fine meshes near $Z/L = 1$; however, the results from the medium and fine meshes are very close to each other (maximum deviation is 0.073% at $Z/L = 1$). Based on these results and others (see [21]), it was decided to use the medium mesh in all calculations.

Experimental results were obtained by Bowers and Mudawar [22] for heat sinks with circular mini-channels (2.54-mm diameter) and micro-channels (510 μm diameter). Most of these results related to boiling conditions; however, some limited single-phase heat transfer data were included. The single-phase data correspond to a single flow rate (i.e., a single Re) for each heat sink with varying input (electrical) heat flux, q''. Numerical results based on the present model were obtained for exactly the same sink geometries and operating conditions reported in [22]. A comparison between the two sets of results is shown in Fig. 4(a). These results are in terms of q'' versus ΔT, where ΔT is the difference between the wall temperature at the top of the fluid channel (midway along the channel) and the inlet fluid temperature. Fig. 4(a) shows that the numerical model predicts the correct trends in terms of the effect of q'' on ΔT, and in terms of the improved performance of the micro-channel over the mini-channel (lower ΔT for the same q''). In order to assess the experimental uncertainty in q'', the actual

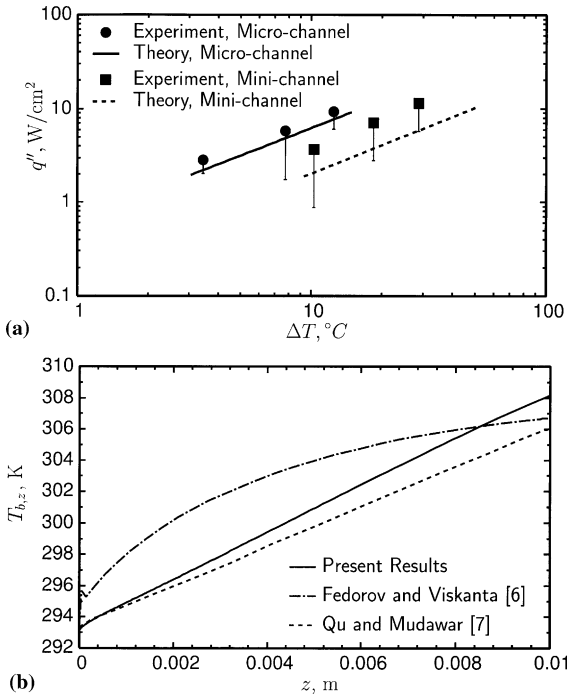

Fig. 4. (a) Comparison with Bowers and Mudawar [22]. (b) Predicted bulk temperature for the test conditions of Kawano et al. [8].

amount of sensible heat gained by the fluid was calculated from data on the bulk-temperature rise, given in Fig. 2(a) and (b) of [22]. The magnitude of q'' calculated from the gain in sensible heat was always lower than q'' measured electrically. The difference between the two values of q'' is indicated by the error bars in Fig. 4(a). The predictions of the present model can be seen in Fig. 4(a) to be within the error bars of the experimental data.

A comparison was also made between the present model and the data of Kawano et al. [8] for the overall friction factor and the overall thermal resistance of a heat sink with rectangular micro-channels. This comparison (documented in [21]) has shown that the present numerical results, as well as those in [6,7], are in agreement with the data within experimental uncertainty. The shape of the axial variation of bulk temperature, $T_{b,z}$, was computed in this comparison and it is shown in Fig. 4(b), together with the predictions from [6,7]. The value of $T_{b,z}$ was calculated from:

$$T_{b,z} = \frac{\int_0^{A_c} wT\,dA_c}{(\pi/4)D^2 w_m} \tag{10}$$

It may be noted from Fig. 4(b) that Fedorov and Viskanta [6], and Qu and Mudawar [7] predicted a considerably different form for the axial variation of bulk temperature at the same operating conditions. The trend predicted by the present model is closer to that in [7]. All three models predict a bulk-temperature gradient that is high near the inlet and continuously decreasing along z. However, Fedorov and Viskanta [6] predict much higher gradients near the inlet and much lower gradients near the exit than the other two models.

4. Results and discussion

Results were obtained for 36 cases, all corresponding to $L/D = 20$, $S/H = 0.5$, and $Pr = 7$ (water). The parametric variation covered the following range of conditions: $H/D = 2$, 3, and 4, $B/D = 1.2$, 1.6, and 2.0, $Re = 500$ and 1000, and $k_s/k_f = 668.3$ (copper–water) and 247.9 (silicon–water). Effects of these parameters on different aspects of the thermal behavior of the heat sink are presented and discussed in this section.

4.1. Wall temperature

An important design feature is the temperature variation on the top (heated) surface of the sink. A uniform temperature on this surface is preferable in order to avoid hotspots on the microchip, resulting in damage, failure, or incorrect data. Fig. 5(a) illustrates the effect of the separating distance between the channels

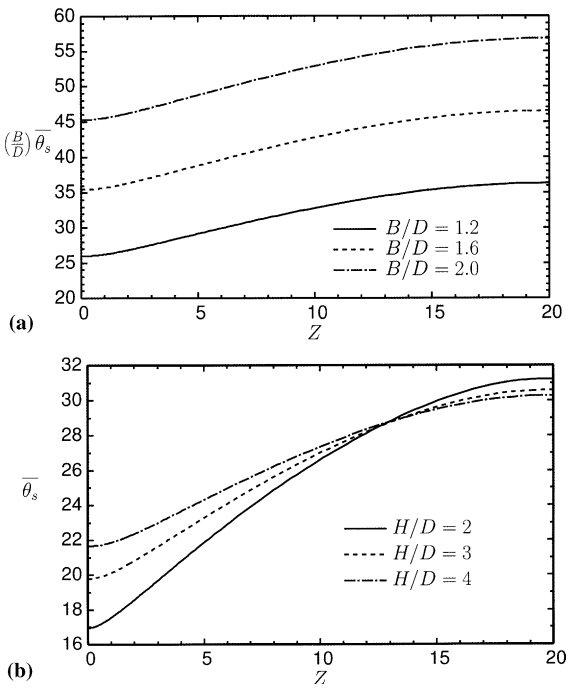

Fig. 5. (a) Effect of B/D on $(\overline{T}_s - T_{in})$ along the top surface for $H/D = 4$, $Re = 500$, and $k_s/k_f = 668.3$. (b) Effect of H/D on $\bar{\theta}_s$ along the top surface for $B/D = 1.2$, $Re = 500$, and $k_s/k_f = 668.3$.

(represented by the ratio B/D) on the temperature at the heated surface (represented by $(B/D)\bar{\theta}_s$), where $\bar{\theta}_s$ is the x-averaged dimensionless temperature at $y = H$. The quantity $(B/D)\bar{\theta}_s (= (\overline{T}_s - T_{in})/(q''D/k_s))$ would isolate the effect of B on $\overline{T}_s$ when all other parameters are held constant. The results in Fig. 5(a), corresponding to $H/D = 4$, $Re = 500$, and $k_s/k_f = 668.3$, show a significant variation in the top-surface temperature along z for all values of B/D. The magnitude of $(\overline{T}_s - T_{in})$ decreases significantly as B/D decreases, consistent with the expectation that smaller B/D results in more efficient heat sinks. The rise in $\overline{T}_s$ from inlet to outlet appears to increase slightly as B/D increases.

The effect of the sink's thickness (represented by H/D) on the value of $\bar{\theta}_s$ at the top-surface is shown in Fig. 5(b) for $B/D = 1.2$, $Re = 500$, and $k_s/k_f = 668.3$. These results show that the surface temperature becomes more uniform as the sink's thickness increases. This may be attributed to increased axial conduction through the solid (back heating) as H/D increases, particularly near the inlet where the boundary layer thickness in the fluid is small.

The effects of Re and k_s/k_f on the value of $\bar{\theta}_s$ at the top-surface are shown in Fig. 6(a) and (b), respectively, for $B/D = 1.2$ and $H/D = 4$. These results confirm the expected trends of decreasing $(\overline{T}_s - T_{in})$ with increasing Re and/or k_s/k_f. An additional effect of increasing k_s/k_f is

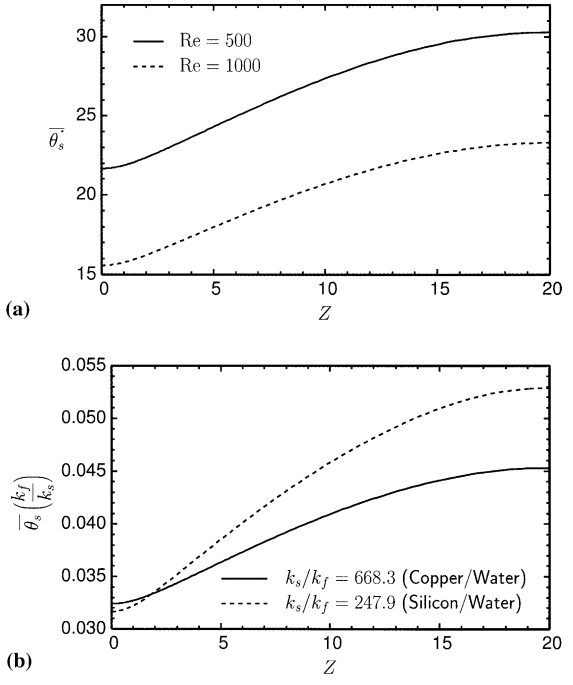

Fig. 6. (a) Effect of Re on $\bar{\theta}_s$ along the top surface of a heat sink with $B/D = 1.2$, $H/D = 4$, and $k_s/k_f = 668.3$. (b) Effect of k_s/k_f on $\theta_s \cdot k_f/k_s$ along the top surface of a heat sink with $B/D = 1.2$, $H/D = 4$, and $Re = 500$.

that the temperature becomes more uniform along the top surface as a result of increased axial conduction in the solid.

4.2. Heat input to the fluid

The heat input to the fluid per unit length, q_z, can be expressed as

$$q_z = (\pi/4)D^2 \rho w_m C_p (\mathrm{d}T_{b,z}/\mathrm{d}z) \tag{11}$$

Eq. (11) can be written in the following dimensionless form:

$$\left(\frac{q_z}{q''B}\right) = \left(\frac{\pi}{4}\right)\left(\frac{k_f}{k_s}\right) Re\ Pr \left(\frac{\mathrm{d}\theta_b}{\mathrm{d}Z}\right) \tag{12}$$

where θ_b is the local dimensionless bulk temperature of the fluid. The quantity $q_z/(q'' \cdot B)$ in Eq. (12) represents the ratio of the heat gained by the fluid per unit length to the heat input at the top surface of the sink per unit length. From an overall energy balance, the axial average of this quantity should be equal to 1.

The results in Fig. 7(a)–(c) indicate that the heat input to the sink per unit length ($q'' B$) experiences a significant redistribution in the axial direction before being absorbed by the coolant. The value of q_z is high at the inlet and decreases continuously along z. This is consistent with the fact that the boundary layer thickness, and therefore the thermal resistance, is low at inlet and increases continuously along z. Fig. 7(a)–(c) show that this phenomenon of axial redistribution of input heat (or back-heating) is further enhanced with increases in B/D and/or H/D (i.e., with more solid volume relative to the fluid volume), or an increase in k_s/k_f (i.e., an increase in the solid conductivity). The effect of increasing Re from 500 to 1000 on the value of $q_z/(q'' \cdot B)$ was studied; however, this effect was found to be small [21].

4.3. Bulk temperature

Based on the behavior of q_z presented above, it is expected that the axial gradient of θ_b will be high at the inlet of the channel and that it will decrease continuously along z. As well, the value of $\mathrm{d}\theta_b/\mathrm{d}Z$ at inlet is expected to increase with increases in B/D, H/D, or k_s/k_f. It should be pointed out that the dimensionless bulk temperature at the channel exit can be formulated as

$$\theta_{b,out} = \left(\frac{4}{\pi}\right)\left(\frac{L}{D}\right)\left(\frac{k_s}{k_f}\right)\left(\frac{1}{Re\,Pr}\right) \tag{13}$$

Thus, $\theta_{b,out}$ is independent of the geometrical parameters B/D and H/D. However, the value of θ_b within $0<(z/L)<1$ is expected to depend on geometry and thermal conductivity of the solid.

Fig. 8(a) and (b) confirm the expected behavior mentioned above. Qualitatively, this form of axial variation of θ_b along z is consistent with the results obtained by Qu and Mudawar [7]. Fedorov and Viskanta [6]

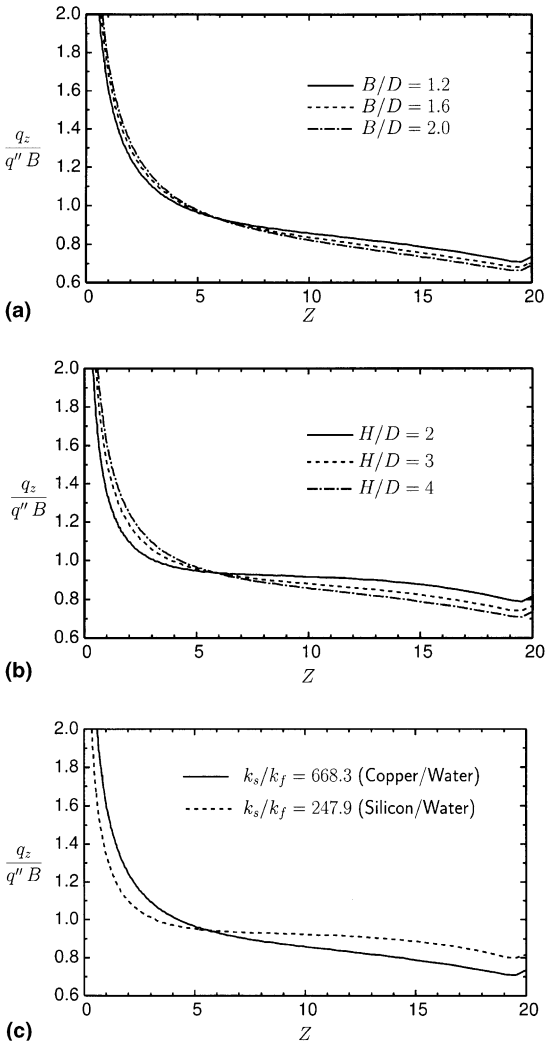

Fig. 7. (a) Effect of B/D on the axial variation of q_z for $H/D = 4$, $Re = 500$, and $k_s/k_f = 668.3$. (b) Effect of H/D on the axial variation of q_z for $B/D = 1.2$, $Re = 500$, and $k_s/k_f = 668.3$. (c) Effect of k_s/k_f on the axial variation of q_z for $B/D = 1.2$, $H/D = 4$, and $Re = 500$.

predicted similar trends but with much steeper θ_b -gradients near the inlet and much flatter gradients near the outlet.

4.4. Angular variation of heat flux at the channel wall

A sample of the results for the angular variation of the local heat flux at the micro-channel's wall, q_i'', is shown in Fig. 9 for $H/D = 4$, $Re = 500$, and $k_s/k_f = 668.3$. These results are presented in terms of $\left[\frac{q_i''}{q''} \cdot \frac{\pi}{(B/D)}\right]$ versus ϕ, and therefore a constant value of 1 on the vertical axis would mean that all the heat input at the top of the channel has been absorbed uniformly around the channel.

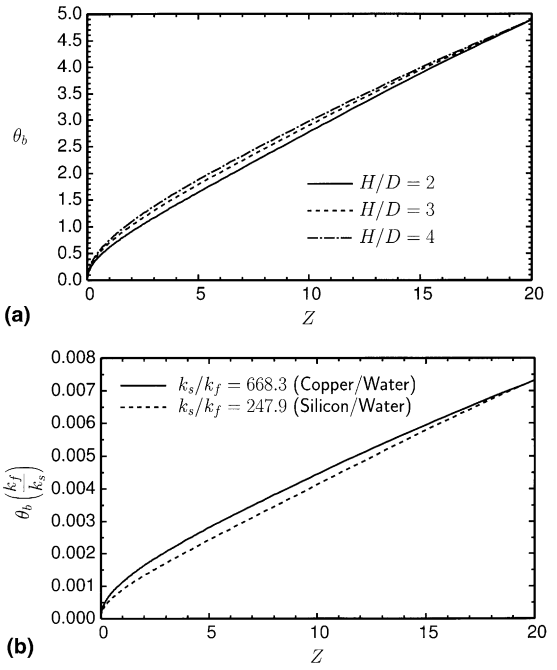

Fig. 8. (a) Effect of H/D on θ_b for $B/D = 1.2$, $Re = 500$, and $k_s/k_f = 668.3$. (b) Effect of k_s/k_f on $(\theta_b \cdot k_f/k_s)$ for $B/D = 1.2$ and $H/D = 4$.

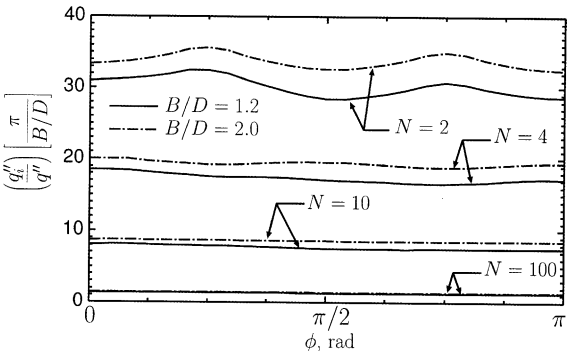

Fig. 9. Angular distribution of heat flux at micro-channel wall ($N = 2$, 4, 10, and 100 correspond to $z/L = 2.24\times10^{-4}$, 7.02×10^{-4}, 2.28×10^{-3}, and 8.77×10^{-2}, respectively).

The results in Fig. 9 illustrate a number of interesting features. First, the heat flux does not vary substantially around the channel, even for $B/D = 1.2$ where the distance between the channels is fairly small. Secondly, back-heating is evident near the channel inlet from values on the vertical axis that are much higher than 1. Finally, back-heating intensifies as B/D increases, consistent with the earlier results presented in Fig. 7(a). Other results reported in [21] confirm that q_i'' increases near the channel inlet with increases in H/D and/or

k_s/k_f, consistent with the results in Fig. 7(b) and (c), respectively.

4.5. Nusselt number

The axial variation of the averaged Nusselt number within the channel cross-section, Nu_z, was calculated and these results are presented in Fig. 10(a) and (b). The value of Nu_z was calculated from

$$Nu_z = \frac{\overline{q''_i} \cdot D}{(\overline{T}_{s,i} - T_b) \cdot k_f} \tag{14}$$

where $\overline{q''_i}$, $\overline{T}_{s,i}$, and T_b are the average heat flux at the solid–fluid interface, the average temperature at the solid-fluid interface, and the bulk temperature, respectively, all evaluated at the same axial location z. Values of Nu_z are plotted against Z^+ in Fig. 10(a) and (b), where

$$Z^+ = \frac{z}{D \cdot Re \cdot Pr} \tag{15}$$

These results correspond to $Re = 500$, $Pr = 7$ (water), and $k_s/k_f = 668.3$ (copper–water). Fig. 10(a) shows results for $B/D = 2$ and $H/D = 4$ (largest solid volume case), while Fig. 10(b) shows results for $B/D = 1.2$ and $H/D = 2$ (smallest solid volume case). In both cases, the computed values of Nu_z are compared with the classical solutions for developing forced convection in tubes with constant wall heat flux and constant wall temperature [23].

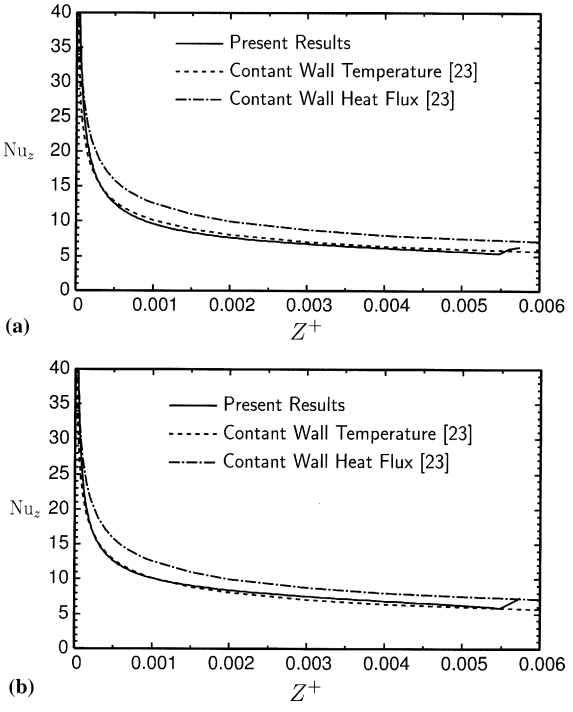

Fig. 10. (a) Axial variation of Nu_z for a micro-channel with $B/D = 2$ and $H/D = 4$ (largest solid volume case). (b) Axial variation of Nu_z for a micro-channel with $B/D = 1.2$ and $H/D = 2$ (smallest solid volume case).

Fig. 10(a) and (b) show that the present values of Nu_z for both solid volume cases follow closely the classical solution for forced convection in tubes with constant wall temperature. The maximum deviation between the present results and the classical solution were about 5% for the largest volume case and about 7% for the smallest volume case. This result is not surprising in view of the large axial variation in $\overline{q''_i}$ that can be inferred from the results in, Figs. 7(a)–(c) and 9. As well, this behavior is consistent with the experimental results of Owhaib and Palm [3] who found that the classical correlations for Nusselt number with a constant-wall-temperature boundary condition were in good agreement with their measurements in both the laminar and turbulent regions.

4.6. Overall thermal resistance

The overall thermal resistance of the heat sink is normally defined as

$$\gamma = \frac{\overline{T}_s(y = H, z = L) - T_{in}}{q'' B_T L} \tag{16}$$

where $\overline{T}_s(y = H,\ z = L)$ is the average wall temperature over the distance $0 \leqslant x \leqslant B$ evaluated at $y = H$ and $z = L$. Eq. (16) can be written in the following non-dimensional form:

$$\Gamma = D \cdot k_f \cdot \gamma = \frac{\overline{T}_s(y = H, z = L) - T_{in}}{\left(\frac{q'' D}{k_f}\right) \cdot \left(\frac{L}{D}\right) \cdot \left(\frac{B_T}{D}\right)} \tag{17}$$

Thus, Γ provides a dimensionless measure for the overall thermal resistance of the heat sink for given values of L/D and B_T/D. Definition (17) allows the study of the effects of the independent parameters B/D, H/D, Re, and k_s/k_f on the overall thermal resistance.

Values of Γ were calculated for $B_T/D = 24$, $S/H = 0.5$, $L/D = 20$, and $Pr = 7$. Table 1 gives a listing of Γ for various values of the independent parameters. These results indicate that the thermal resistance decreases significantly as B/D (which is a measure of the separating distance between the micro-channels) decreases. This trend is consistent with the data in Fig. 8 showing that the magnitude of $(\overline{T}_s - T_{in})$ decreases significantly as B/D decreases. As well, this result is similar to the trend reported by Weisberg et al. [14] for rectangular micro-channels. For the range covered in Table 1, Γ decreases by 34–36% as B/D decreases from 2.0 to 1.2. The parameter H/D relates to the thickness of the heat sink and Table 1 indicates that there is a small change in Γ within the range $2 \leqslant H/D \leqslant 4$. The effect of H/D on the wall temperature, presented in Fig. 5(b), indicates that H/D has a significant effect on $(\overline{T}_s - T_{in})$ at the channel inlet,

Table 1
Values of $\Gamma\times10^4$

		Re = 500			Re = 1000		
k_s/k_f	B/D	H/D = 2	H/D = 3	H/D = 4	H/D = 2	H/D = 3	H/D = 4
247.9	1.2	1.31	1.31	1.33	1.01	1.03	1.05
	1.6	1.63	1.63	1.65	1.25	1.27	1.29
	2.0	1.98	1.98	1.98	1.51	1.53	1.53
668.3	1.2	1.17	1.14	1.13	0.890	0.875	0.868
	1.6	1.50	1.47	1.45	1.14	1.11	1.11
	2.0	1.83	1.79	1.77	1.38	1.35	1.35

while at the channel outlet the effect is small. Therefore, increasing H/D has the advantage of making $(\overline{T}_s - T_{in})$ more uniform along the heat sink without sacrificing much on Γ. Weisberg et al. predicted a small increase in thermal resistance with the substrate thickness.

Table 1 also shows that Re has a significant effect on Γ, whereby Γ increases by 30–33% as Re decreases from 1000 to 500. Again, this trend is consistent with the results shown earlier in Fig. 6(a). Finally, k_s/k_f has the predicted effect on Γ; a decrease in Γ as k_s/k_f increases, which is also consistent with the wall-temperature results shown in Fig. 6(b).

4.7. Comparison with heat sinks with rectangular micro-channels

Because most of the previous studies on micro-channel heat sinks have focused on the rectangular geometry, it was decided to compare the performance of the circular and rectangular shapes in terms of overall thermal resistance and pumping power. Fig. 11(a) shows a schematic diagram of the unit rectangular cell considered in this comparison with channel dimensions $L_1\times L_2$. The comparison was based on equal hydraulic diameter, D_h, and equal Reynolds number, Re, for both shapes. Therefore,

$$\frac{D_h}{D} = \frac{2(L_1/D)(L_2/D)}{(L_1/D)+(L_2/D)} = 1 \tag{18}$$

The condition of equal Re results in equal w_m in both channels.

Computations were conducted for three values of the aspect ratio α $(= L_2/L_1)$ with the following conditions for both channels: B/D = 1.2, H/D = 4, S/H = 0.5, L/D = 20, B_T/D = 24, Re = 500, Pr = 7, and k_s/k_f = 668.3. Mesh independence was verified for the rectangular-channel results. The mesh for the channel with α = 1 had 1351 control volumes in each cross-section and a total of 271,551 control volumes in the three-dimensional domain, while the mesh for the channel with α = 5 had 1394 control volumes in each cross-section and a total of 280,194 control volumes in the three-dimensional domain. The pumping power was calculated from:

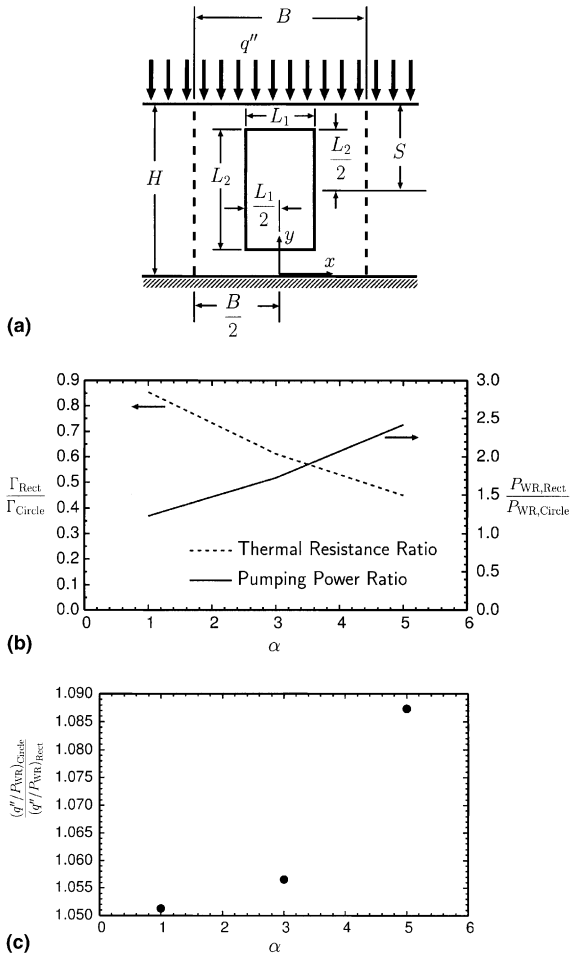

Fig. 11. (a) Schematic diagram of a rectangular unit cell. (b) Comparison between rectangular and circular channels in terms of Γ and P_{WR}. (c) Comparison between rectangular and circular channels in terms of rate of heat dissipation per unit pumping power.

$$P_{WR} = N \cdot A_c \cdot w_m(p_{in} - p_{out}) \tag{19}$$

with the cross-sectional area $A_c = L_1\times L_2$ for the rectangular channel and $A_c = (\pi/4)D^2$ for the circular channel.

Fig. 11(b) shows the Γ-ratio as well as the P_{WR}-ratio of the rectangular channel relative to the circular channel for $1 \leqslant \alpha \leqslant 5$. It is evident from these results that the thermal performance of the rectangular channels is superior, particularly at large α. On the other hand, the pumping-power requirement is less favorable for the rectangular channel, particularly at large α. The ratio of surface area to cross-sectional area is higher for the rectangular channels than the circular ones, and this may be the reason for the rectangular channels to have higher heat transfer as well as higher pressure drop.

Another parameter that may be important in some applications is the rate of heat dissipation per unit pumping power, $(L \cdot B_T \cdot q''/P_{WR})$. A comparison between the rectangular and circular channels was conducted in terms of this parameter and the results are shown in Fig. 11(c); the two channels have equal L and equal B_T. Within the range $1 \leqslant \alpha \leqslant 5$, the circular channel is capable of dissipating more heat per unit pumping power than the rectangular channel under the specified conditions for the present comparison (equal D_h and equal Re).

5. Conclusions

Three-dimensional fluid flow and conjugate heat transfer in heat sinks with circular micro-channels have been analyzed numerically. The analysis uses the continuum model, which includes the conventional Navier–Stokes equations and the conventional energy equation. The validity of this approach has been demonstrated by comparisons with existing experimental data. Results were generated for the detailed description of the local and average heat transfer characteristics including wall and fluid temperatures, heat flux, Nusselt number, and overall thermal resistance. Effects of the heat-sink geometry (B/D and H/D), Reynolds number (Re), and thermal conductivity of the solid substrate (k_s/k_f) were presented and discussed. Furthermore, a comparison between the performances of heat sinks with circular and rectangular channels was conducted. The following conclusions can be drawn from the present results:

1. A significant variation exists in the top-surface temperature along z for all the cases considered. The magnitude of $(\overline{T}_s - T_{in})$ decreases significantly with a decrease in B/D, or an increase in H/D, Re or k_s/k_f. In addition, increases in H/D or k_s/k_f were found to induce uniformity in the top-surface temperature. Temperature variation within the solid substrate cross-section was found to be small in all cases.
2. Significant back-heating was noted, which resulted in high values of q_z at the inlet and a continuous decrease in q_z along z. This phenomenon of back-heating intensifies with increases in B/D, H/D, or k_s/k_f. Consequently, the axial gradient of the bulk temperature was found to be high at the inlet of the channel and it decreased continuously along z. The value of $d\theta_b/dZ$ at inlet was found to increase with increases in B/D, H/D, or k_s/k_f.
3. The heat flux at the wall of the micro-channel does not vary substantially in the circumferential direction; however, it varies significantly in the axial direction. This behavior was found to be true for the whole range of independent parameters covered in the study.
4. The axial variation of Nusselt number was found to follow closely the classical solution for forced convection in tubes with constant wall temperature. This behavior was found to be true for two extreme cases of the heat sink geometry.
5. The overall thermal resistance of the heat sink was found to decrease significantly with a decrease in B/D, or an increase in Re and/or k_s/k_f. The parameter H/D, which relates to the thickness of the heat sink, had a small effect on the overall thermal resistance within the range $2 \leqslant H/D \leqslant 4$.
6. On the basis of equal hydraulic diameter and equal Reynolds number, heat sinks with rectangular channels were found to have less thermal resistance but require more pumping power than heat sinks with circular channels. In terms of rate of heat dissipation per unit pumping power, the circular geometry gave a slightly better performance (up to 9% higher at $\alpha = 5$).

Acknowledgment

The financial assistance provided by the Natural Sciences and Engineering Research Council of Canada is gratefully acknowledged.

References

[1] S.G. Kandlikar, W.J. Grande, Evolution of microchannel flow passages—thermohydraulic performance and fabrication technology, Heat Transfer Eng. 24 (2003) 3–17.
[2] T.M. Adams, S.I. Abdel-Khalik, S.M. Jeter, Z.H. Qureshi, An experimental investigation of single-phase forced convection in microchannels, Int. J. Heat Mass Transfer 41 (1998) 851–857.
[3] W. Owhaib, B. Palm, Experimental investigation of single-phase convective heat transfer in circular microchannels, Exp. Thermal Fluid Sci. 28 (2004) 105–110.
[4] Z.-Y. Guo, Z.-X. Li, Size effect on microscale single-phase flow and heat transfer, Int. J. Heat Mass Transfer 46 (2003) 149–159.

[5] P. Gao, S. Le Person, M. Favre-Marinet, Scale effects on hydrodynamics and heat transfer in two-dimensional mini and microchannels, Int. J. Thermal Sci. 41 (2002) 1017–1027.
[6] A.G. Fedorov, R. Viskanta, Three-dimensional conjugate heat transfer in the microchannel heat sink for electronic packaging, Int. J. Heat Mass Transfer 43 (2000) 399–415.
[7] W. Qu, I. Mudawar, Analysis of three-dimensional heat transfer in micro-channel heat sinks, Int. J. Heat Mass Transfer 45 (2002) 3973–3985.
[8] K. Kawano, K. Minakami, H. Iwasaki, M. Ishizuka, Development of micro channels heat exchanging, in: Application of Heat Transfer in Equipment, Systems, and EducationASME HTD-Vol. 361-3/PID-Vol. 3, 1998, pp. 173–180.
[9] K.C. Toh, X.Y. Chen, J.C. Chai, Numerical computation of fluid flow and heat transfer in microchannels, Int. J. Heat Mass Transfer 45 (2002) 5133–5141.
[10] D.B. Tuckerman, Heat transfer microstructures for integrated circuits, Ph.D. Thesis, Stanford University, Stanford, California, 1984.
[11] W. Qu, I. Mudawar, Experimental and numerical study of pressure drop and heat transfer in a single-phase microchannel heat sink, Int. J. Heat Mass Transfer 45 (2002) 2549–2565.
[12] K.K. Ambatipudi, M.M. Rahman, Analysis of conjugate heat transfer in microchannel heat sinks, Numer. Heat Transfer (Part A) 37 (2000) 711–731.
[13] T.M. Harms, M. Kazmierczak, F.M. Gerner, A. Holke, H.T. Henderson, J. Pilchowski, K. Baker, Experimental investigation of heat transfer and pressure drop through deep microchannels in a (1 1 0) silicon substrate, ASME-HTD 351 (1997) 347–357.
[14] A. Weisberg, H.H. Bau, J.N. Zemel, Analysis of microchannels for integrated cooling, Int. J. Heat Mass Transfer 35 (1992) 2465–2474.
[15] G. Tunc, Y. Bayazitoglu, Heat transfer in rectangular microchannels, Int. J. Heat Mass Transfer 45 (2002) 765–773.
[16] Gh.M. Mala, D. Li, Flow characteristics of water in microtubes, Int. J. Heat Fluid Flow 20 (1999) 142–148.
[17] J.H. Ryu, D.H. Choi, S.J. Kim, Numerical optimization of the thermal performance of a microchannel heat sink, Int. J. Heat Mass Transfer 45 (2002) 2823–2827.
[18] S.V. Patankar, Numerical Heat Transfer and Fluid Flow, Hemisphere, New York, 1980.
[19] C. Prakash, S.V. Patankar, A control-volume-based finite-element method for solving the Navier–Stokes equations using equal-order velocity-pressure interpolation, Numer. Heat Transfer 8 (1985) 259–280.
[20] G.E. Schneider, M.J. Raw, Control-volume finite-element method for heat transfer and fluid flow using co-located variables—1. Computational procedure, Numer. Heat Transfer 11 (1987) 363–390.
[21] C.J. Kroeker, Three-dimensional thermal analysis of heat sinks with circular microchannels, M.Sc. Thesis, University of Manitoba, Winnipeg, Manitoba, Canada, 2003.
[22] M.B. Bowers, I. Mudawar, High flux boiling in low flow rate, low pressure drop mini-channel and micro-channel heat sinks, Int. J. Heat Mass Transfer 37 (1994) 321–332.
[23] R.K. Shah, A.L. London, Laminar Flow Forced Convection in Ducts, Academic Press, New York, 1978.